CONTINUOUS-TIME FIR FILTERS AT MICROWAVE FREQUENCIES

Shanthi Pavan
Department of Electrical Engineering
Indian Institute of Technology, Madras
Chennai 600 036, India
shanthi@ee.iitm.ernet.in

ABSTRACT

We discuss adaptive FIR filters operating in the continuous time domain. These filters become attractive to implement at microwave frequencies. The traveling wave FIR filter topology is compared with a conventional tapped delay line, and its advantages when used as an adaptive equalizer are pointed out.

1. INTRODUCTION

Rapid scaling of bandwidth in optical networks have resulted in deployment of Optical Time Division Multiplexed Systems (OTDM) with bit rates as high as 10 and 40 Gbps. At these data rates, there are significant link penalties associated with optical fiber impairments like chromatic dispersion and polarization mode dispersion (PMD). While techniques do exist to correct for these impairments, they work in the optical domain. Electronic solutions to the problem are attractive due to their potential low cost. Since fiber impairments vary with environmental conditions, these solutions will necessarily have to be adaptive. It is in this context that adaptive electronic equalizers are used. By now, equalization as a technique is very well known and equalizers of high complexity are routinely used in most channels, ranging from telephony to hard disk drives. While the optical channel is more "benign" when compared to some of the channels referred to above, the main challenge lies in being able to implement these well known DSP techniques at speeds of several tens of gigabits per second [1].

The block diagram of a typical fiber optic receiver employing an adaptive equalizer is shown in Figure 1, where the equalizer and the clock and data recovery (CDR) unit are shown together. Figure 2(a) shows an all digital implementation of the equalizer/CDR, which is very popular in low speed channels. The signal is sampled and quantized by an analog-to-digital converter (ADC) before equalization. Often, the signal is sampled at twice the symbol rate, so as to implement a matched filter-symbol spaced equalizer combination. The resolution required of the ADC is governed by the SNR required at the decision device and the coefficients of the FIR filter (which in turn depend on the channel response). Convergence of the equalizer taps is coupled with the dynamics of the timing recovery loop. This architecture poses many problems at bit rates of several Gbps. Implementing a high speed ADC is far from trivial, and might require excessive parallelism. In order to prevent timing mismatch between several parallel paths, a front end sample-and-hold operating at the symbol rate is required. A fractionally spaced implementation is only likely to worsen the above problems. The digital FIR filter would also involve massive parallelism and pipelining, making the whole receiver a very power hungry one. In its defense, however, improvements in IC fabrication technology will tend to make this increasingly feasible, and this architecture might be the one of choice in the future.

Figure 2(b) shows an *all analog* approach to the equalization problem. Here, a physical delay element, such as a transmission line is used to produce delayed replicas of the input. While such an approach would lead to physically very large equalizers at low frequencies, it becomes attractive at very high speeds. Since the delay elements are passive, they dissipate no power. This opens up the possibility of implementing very low power equalizers operating at several gigabits per second. Moreover, the delay Td can be made $T/2$ without any problem. These types of filters, referred to as continuous-time FIR filters are analyzed in this paper. In Section 2, we consider a conventional tapped delay line structure, as inspired from DSP. The effects of impedance mismatch at the ends of the transmission line, and uniformly distributed series loss are analyzed. The traveling wave FIR filter topology, and its advantages relative to a conventional tapped delay line structure are discussed in Section 3. Tap weight adaptation issues discussed in Section 4. Simulation results are presented in Section 5 and conclusions are given in Section 6.

2. TOPOLOGICAL CONSIDERATIONS

We draw our inspiration from discrete time FIR filters to arrive at the analog FIR filter topology shown in Figure 3, which, for illustrative purposes has three taps. The delays are implemented using transmission lines with a characteristic impedance of Z_o and length T seconds. A transconductor of value G is used to convert the input voltage to a current, which drives the delay line. Taps are implemented by transconductors with values w_1, w_2 & w_3 as shown. Summation of the tapped signals is done in the current domain, and the output voltage is developed across a load resistor of

value $0.5R_T$ (this particular value is chosen in order to facilitate comparison with another topology, and will become clear shortly.) The impulse response (Figure 3) of the filter can be expressed as

$$h(t) = (R_T/2)(w_1 h_{v1}(t) + w_2 h_{v2}(t) + w_3 h_{v3}(t)) \quad (1)$$

where $h_{v1}(t), h_{v2}(t)$ & $h_{v3}(t)$ are the impulse responses at nodes $v1$, $v2$ and $v3$ respectively. If $R_T = Z_o$,

$$h(t) = G\left[\frac{Z_o}{2}\right]^2 (w_1\,\delta(t) + w_2\,\delta(t-T) + w_3\,\delta(t-2T)) \quad (2)$$

In practice, impedance mismatch at the ends of the delay line will cause reflections. We denote the reflection coefficient by Γ_T, which is approximately $(R_T - Z_o)/(2Z_o)$. $h_{v1}(t)$, $h_{v2}(t)$ and $h_{v3}(t)$ are modified due to reflections as shown in Figure 3. For cases of practical interest, Γ_T will be small compared to unity, so terms of the order of Γ_T^2 and higher can be safely neglected. The impulse response of the filter is

$$\begin{aligned} h(t) \quad \approx \quad & G(\frac{Z_o}{2})^2(1+3\Gamma_T)(w_1\delta(t) + w_2\delta(t-T) + \\ & w_3\delta(t-2T) + w_2\Gamma_T\delta(t-3T) + \\ & w_1\Gamma_T\delta(t-4T)) \end{aligned} \quad (3)$$

2.1. Series Losses

We now consider the effects of transmission line nonidealities on the impulse response of the filter. The most important among these nonidealities is uniformly distributed series (resistive) loss. In order to build intuition, we model each transmission line with a delay T and a total series loss of R_s by dividing it into N sections. The three tap FIR shown in Figure 3 would now consist of $2N$ transmission line sections, each of characteristic impedance Z_o, delay T/N and lumped series resistance Rs/N. We consider the case when $\Gamma_T = 0$, and the practical situation where $R_s/Z_o << 1$. If a wave of unit magnitude is launched at node $v1$ in the direction shown in Figure 4, we see that a small reflection occurs at the end of the first section after a time T/N. The magnitude of this reflected wave is approximately

$$\Gamma_R = \frac{R_s/N}{2Z_o + R_s/N} \approx \frac{R_s}{2NZ_o} \quad (4)$$

This reflection reaches node $v1$ after a delay T/N, so the total time elapsed since the launching of the initial wave is $2T/N$. The transmitted wave, on the other hand, has a magnitude of $(1-\Gamma_s) \approx 1$, and again undergoes a small reflection at the end of the second section. This reflected wave gets back to node $v1$ after a delay of $4T/N$, and with a magnitude of $\Gamma_s(1-\Gamma_s)^2 \approx \Gamma_s$. The magnitudes of reflections from consequent sections can also be computed in a similar manner. Figure 4(a) shows the bounce diagrams for the case considered above. Note the timescale in this plot. In the limit of infinite N, $h_{v1}(t)$ can be shown to have an exponentially decaying tail, as shown in Figure 4(b). For the case where there is series loss as well as mismatch at the terminations, $h_{v1}(t)$ would look like that shown in Figure 4(c). Impulse responses $h_{v2}(t)$ and $h_{v3}(t)$ can be obtained in a similar manner. Like $h_{v1}(t)$, they would have exponentially decaying tails associated with uniform series loss, and impulses due to reflections at the ends of the line. Note that the amplitude of these tails is proportional to $\frac{R_s}{Z_o}$, which, in practice should be made small (of the order of 0.05).

The key points to note from the discussion in this section are as follows :

1. Reflections at the ends of the delay line cause the filter impulse response to "spill" over its ideal span. If the reflection coefficient is small, then the span of the impulse response with impedance mismatch is about twice the span of the ideal impulse response.

2. Uniform series loss results in exponentially decaying tails appearing in the node impulse responses. If the reflection coefficient associated with the terminating resistors R_T is small, then these tails are also contained within twice the span of the ideal impulse response.

3. It is not possible to constrain the impulse response of the filter to within the span of the ideal filter, by manipulating the tap weights w_1, w_2 and w_3. This is clear from equation (3).

4. From observation (3) above, it is clear that if the filter is used in the context of adaptive equalization to compensate for channel inter symbol interference (ISI), this topology is more likely to worsen the problem than mitigate it.

3. TRAVELING WAVE FIR FILTERS

Consider the filter structure shown in Figure 5. Topologically, it is equivalent to a traveling wave amplifier, but with the output being taken at the "anti-sync" end [2] [3] [4]. While the possibility of using this structure as an FIR filter has been pointed out in the literature, its robustness, especially in the context of adaptive equalization, does not seem to have been adequately appreciated.

The filter has two sections of cascaded transmission lines, one on the input side and one on the output side. The impulse response of the filter is written as

$$h(t) = w_1 h_{w1}(t) + w_2 h_{w2}(t) + w_3 h_{w3}(t) \quad (5)$$

$h_{w1}(t)$ is the impulse response of the filter with $w1 = 1$ and $w2, w3 = 0$. $h_{w2}(t)$ and $h_{w3}(t)$ are similarly defined. These responses are shown in Figure 5, where $h_{v1}(t)$, $h_{v2}(t)$ and $h_{v3}(t)$ are shown on the left. In these plots, all terms of the order of Γ_T^2 and higher have been neglected. It is easily seen that $h_{w1}(t) = h_{v1}(t) * h_{v1}(t)/G$. Since $h_{v1}(t) \approx G(\frac{Z_o}{2})(1+\Gamma_T)(\delta(t) + \Gamma_T\delta(t-2T))$, we have

$$h_{w1}(t) \approx G(\frac{Z_o}{2})^2(1+2\Gamma_T)(\delta(t) + 2\Gamma_T\delta(t-2T)) \quad (6)$$

This is plotted on the right side of Figure 5. Similarly, it can be shown that

$$h_{w2}(t) \approx G(\frac{Z_o}{2})^2(1+2\Gamma_T)(\delta(t-T)+ 2\Gamma_T\delta(t-2T)) \quad (7)$$

$$h_{w3}(t) \approx G(\frac{Z_o}{2})^2(1+2\Gamma_T)\delta(t-2T) \quad (8)$$

Using (5), and the results above, we see that

$$h(t) \approx G(\frac{Z_o}{2})^2(1+2\Gamma_T)(w_1\delta(t)+w_2\delta(t-T)+ (w_3+2\Gamma_T w_1+2\Gamma_T w_2)\delta(t-2T)) \quad (9)$$

We see that

1. If the reflection coefficient is small, then the span of the impulse response with impedance mismatch is *the same* as the span of the ideal impulse response.

2. Reflections cause tap weight "contamination". In the example discussed above, we see that even if $w3$ is set to zero, there is a component of the impulse response at $t = 2T$. This can be corrected by using a modified value for $w3$, which is seen to be $w3' = w3 - 2\Gamma_T w_1 - 2\Gamma_T w_2$.

3. Given that typical reflection coefficients achievable without using special trimming techniques are of the range $|\Gamma_T| < 0.05 - 0.1$, corresponding to resistor mismatch between $10-20\%$, it is seen that a traveling wave FIR structure is at least an order of magnitude improvement over the conventional structure shown in Figure 3, as far as residual induced "ISI" terms outside the equalizer span are concerned.

3.1. Choice of tap spacing, and effect of high frequency conductor and dielectric losses

The tap spacing can be made equal to one-half the symbol rate so that the equalizer implements a matched filter-symbol spaced equalizer cascade. Small variations in tap spacing around the nominal value are not critical, and unlike a digital implementation, no particular penalty is incurred by reducing the tap spacing relative to a symbol interval. The frequency response of the filter with ideal transmission lines is periodic with period $1/T$, but high frequency conductor and dielectric losses (presumably due to skin effect and dielectric relaxation) cause attenuation of the "image" responses. This might actually be to our benefit, as this filters out high frequency noise prior to the sampling operation.

4. TAP WEIGHT ADAPTATION

One of the important properties of an FIR filter is that the derivative of the filter output with respect to a tap weight (gradient signal) is simply a delayed version of the input. This enables simple implementation of the FIR tap weight adaptation loops. Gradient signals are not easily obtained for a traveling wave FIR filter, as is apparent from equation 9. Even in the absence of reflections and series loss, the tap spacing T might change with environmental conditions. Note however, that the filter is still a linear combiner, hence the error surface is unimodal. Efficiently adapting filter coefficients when gradient signals are not available (or are too cumbersome to compute) is an area of active research ([5][6] and references therein). One approach that has been employed in optical channels is to use bit error rate (BER) as the objective function, to be minimized with respect to the tap weights. In many optical receivers BER is either directly available from forward error correction (FEC) blocks. Alternatively, it can be estimated using pseudo-error techniques. Another promising approach [5] that has been demonstrated at low frequencies is estimation of the gradient by dithering individual taps and observing the change in output with respect to each tap.

5. SIMULATION RESULTS

In this section, we present simulation results of a traveling wave FIR equalizer, operating on a 10 Gbps NRZ bit stream passing through a channel $0.5\delta(t)+0.5\delta(t-0.8T_b)$, with $T_b = 100$ ps. The transmit filter is a 4th order Bessel section with a half power bandwidth of 7.5 GHz. The eye diagram at the input of the receiver is shown in Figure 6. The 10 tap equalizer is implemented with elements which exhibit transmission-line like behavior in the frequency range of interest. Tap spacing is 48 ps. R_s/Z_o is about 0.04, and so is Γ_T. Figure 7 shows the eye diagram at the output of the equalizer. The frequency response of the equalizer is shown in Figure 8. Note the boost in the response around 5 GHz.

6. CONCLUSION

We discussed the potential of analog FIR filters operating in the microwave frequency range. In the presence of practical nonidealities like impedance mismatch and series loss, it was shown that the traveling wave FIR filter topology is a big improvement over a conventional tapped delay line filter. Simulation results for a 10 tap equalizer operating on a 10 Gbps NRZ bit stream corrupted by ISI were given.

REFERENCES

[1] K. Azadet et. al, "Equalization and FEC techniques for optical transceivers," IEEE Journal of Solid State Circuits, vol 37, no. 3, pp. 317-27, Mar 2002.

[2] P. Monteiro et. al, "10 Gbps pulse shaping distributed based transversal filter front-end for optical soliton re-

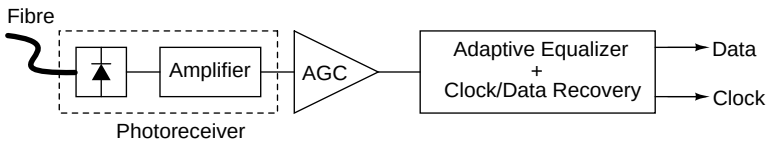

Figure 1: Typical optical receiver employing an adaptive equalizer.

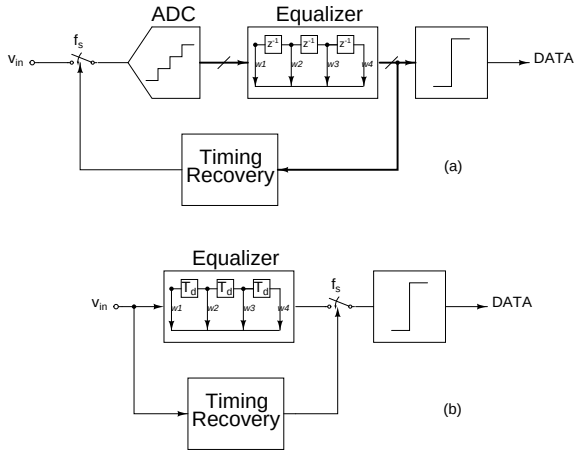

Figure 2: Equalizer architecture approaches.

ceivers," IEEE Microwave and Guided Wave Letters, vol 8, no. 1, pp. 4-6, Jan 1998.

[3] A. Borjak et. al, "High speed generalized distributed-amplifier-based transversal filter topology for optical communication systems," IEEE Trans. on Microwave Theory and Techniques vol 45, no. 8, pp. 1453-7, Aug 1997.

[4] A. Freundorfer et. al, "Adaptive transversal preamplifier for high speed light wave systems," IEEE Microwave and Guided Wave Letters, vol 11, no. 7, pp. 293-5, Jul 2001.

[5] A. Carusone et. al, "Analog Filter Adaptation Using a Dithered Linear Search Algorithm," IEEE Int. Symp. Circuits and Syst., May 2002.

[6] A. Carusone et. al, "Obtaining digital gradient signals for analog adaptive filters," IEEE Int. Symp. Circuits and Syst., May 1999.

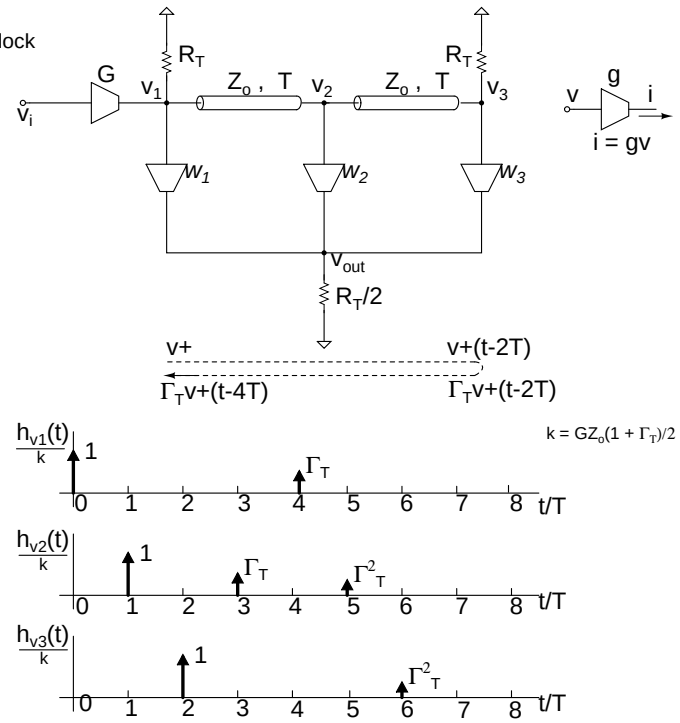

Figure 3: $h_{v1}(t), h_{v2}(t)$ & $h_{v3}(t)$ in the presence of reflections.

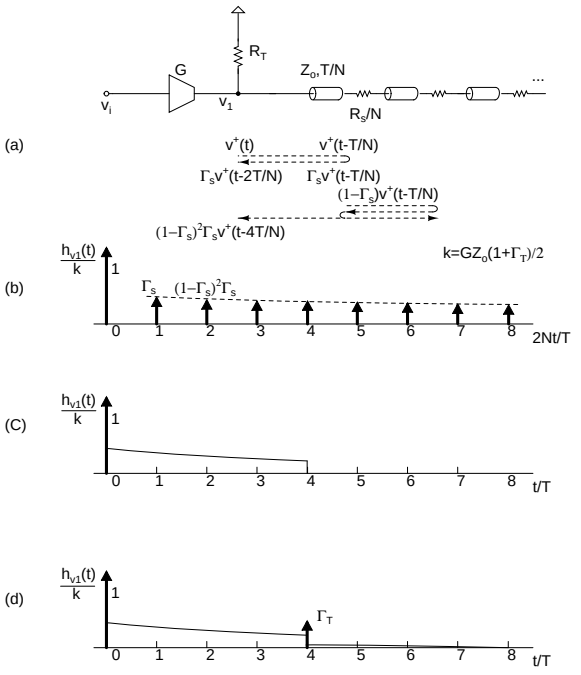

Figure 4: Modeling uniform series loss.

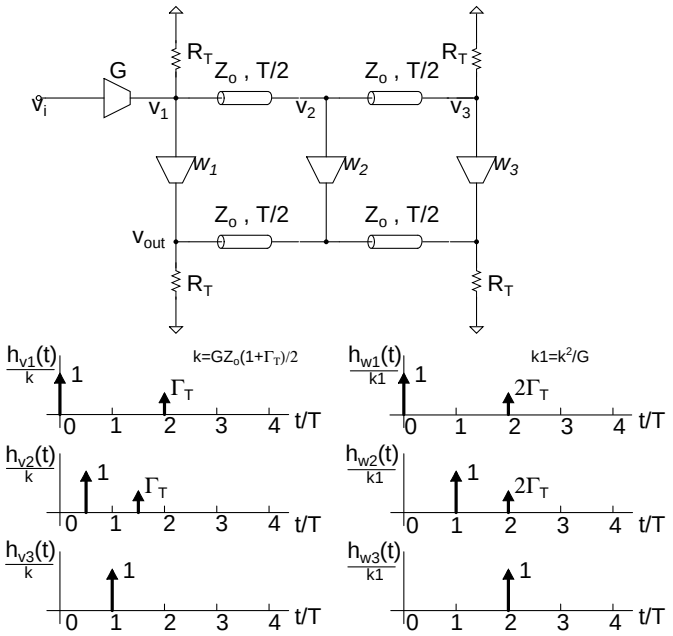

Figure 5: Traveling Wave FIR structure.

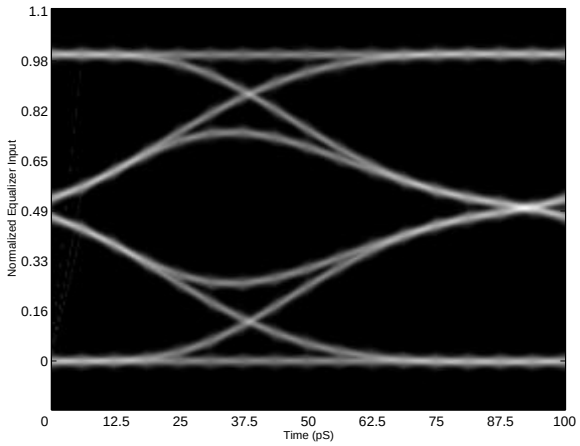

Figure 6: Eye diagram at the equalizer input.

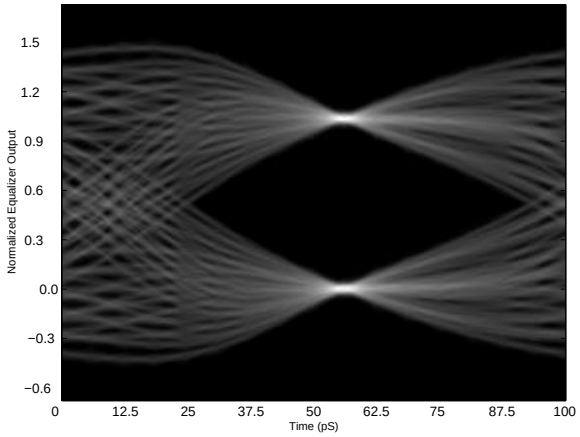

Figure 7: Eye diagram at the equalizer output.

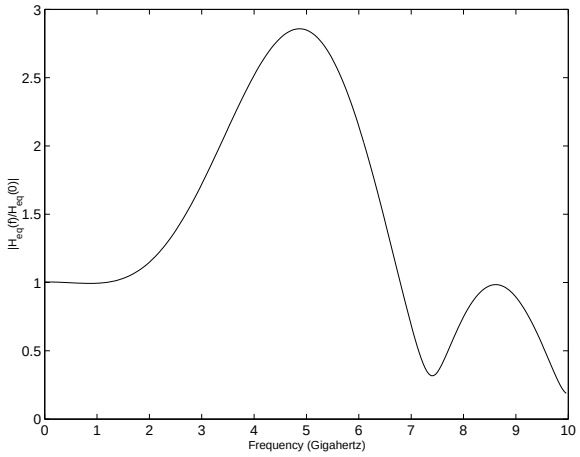

Figure 8: Frequency response of the equalizer.